Hindawi
International Journal of Rotating Machinery
Volume 2017, Article ID 9131275, 10 pages
https://doi.org/10.1155/2017/9131275

*Research Article*

# Influence of Varnish on Bearing Performance and Vibration of Rotating Machinery

**Chu Zhang,[1] Jian-Gang Yang,[2] Shi Liu,[1] Qing-Shui Gao,[1] and Yi Yang[1]**

[1]*Electric Power Research Institute of Guangdong Power Grid Co. Ltd., Guangzhou 510080, China*
[2]*National Engineering Research Center of Turbo-Generator Vibration, Southeast University, Nanjing 210096, China*

Correspondence should be addressed to Chu Zhang; zhangchu718@163.com

Received 18 May 2017; Revised 13 August 2017; Accepted 19 September 2017; Published 19 October 2017

Academic Editor: Ryoichi Samuel Amano



Varnish is a kind of fouling adhered on bearing inner face near the load zone. The model to analyze its influence on bearing performance and rotor vibration was set up. Pressure and temperature distribution were solved on the basis of the Reynolds equation by the iteration method simultaneously. It is found that bearing performance is changed by the step flow effect at the leading edge of the varnish. Its influence is more obvious when the rotating speed is low. Bearing varnish results in a large decrease of minimum clearance and an increase in the oil film temperature and pressure. Loading capacity of bearing is also decreased. It is harmful to the bearing. With the varnish, the minimum oil film thickness decreases. This leads to an increase of bearing stiffness and damping coefficients. Its influence is larger in the horizontal direction than that in the vertical direction. The trend of unbalance response to rotating speed is similar. There is little influence of the varnish on the modal frequency. However, system stability is improved due to the increased bearing damping coefficients.

## 1. Introduction

Journal bearings have a great influence on the safe operation of rotating machinery. Machine works reliably under the squeeze flow effect formed in the convergent gap between bearing inner face and the journal.

With the development of industry, journal surface speed becomes higher and bearing load becomes more and more heavy. Varnish problem has occurred on journal bearings [1]. Varnish is a kind of fouling adhered on journal bearing inner face nearby the load zone, resulting in poor bearing lubrication. It could lead to unacceptable rises in temperature and vibration [1]. Now, the research on the formation mechanism, detection, prevention, and removal of the varnish is being carried out [2]. The formation of varnish is related to the quality of lubricating oil and the condition of journal bearing. The high temperature generated by the variable load operation of bearing will accelerate the formation of the varnish [3].

The clearance of bearing with varnish is irregular. Research on the performance of bearing with irregular clearance is mainly focused on groove or microtexture [4–8]. Bearing performance can be improved through an appropriate arrangement of the textured area on the contact surface [9, 10]. The texture arrangement, mainly the location domain on the journal bearing, is the main criterion for journal bearing performance enhancement. It would be interesting to put dimples in the bearing first angular part (between 0 and 180) which is the maximum pressure region [11]. Appropriately choosing groove length, width, or interval can reduce the maximum radius, collapse pressure, and collapse temperature of the bubble. There exists a critical groove depth minimizing the bubble pressure and temperature [12]. The influence of surface variations such as texturing or grooving on the bearing performances was also compared [13]. The microgrooving reduces the friction coefficient and average temperature is maximum in comparison with spherical texture. Influence of texture distributions on vibration was investigated [14]. Three kinds of textures configurations are designed and applied on the lower pad surface. There is a significant decrease in acceleration amplitude of the textured bearings compared to nontextured bearings.

From inspection results of many bearings, varnish area is larger than expected. Unlike the groove or the microtexture,

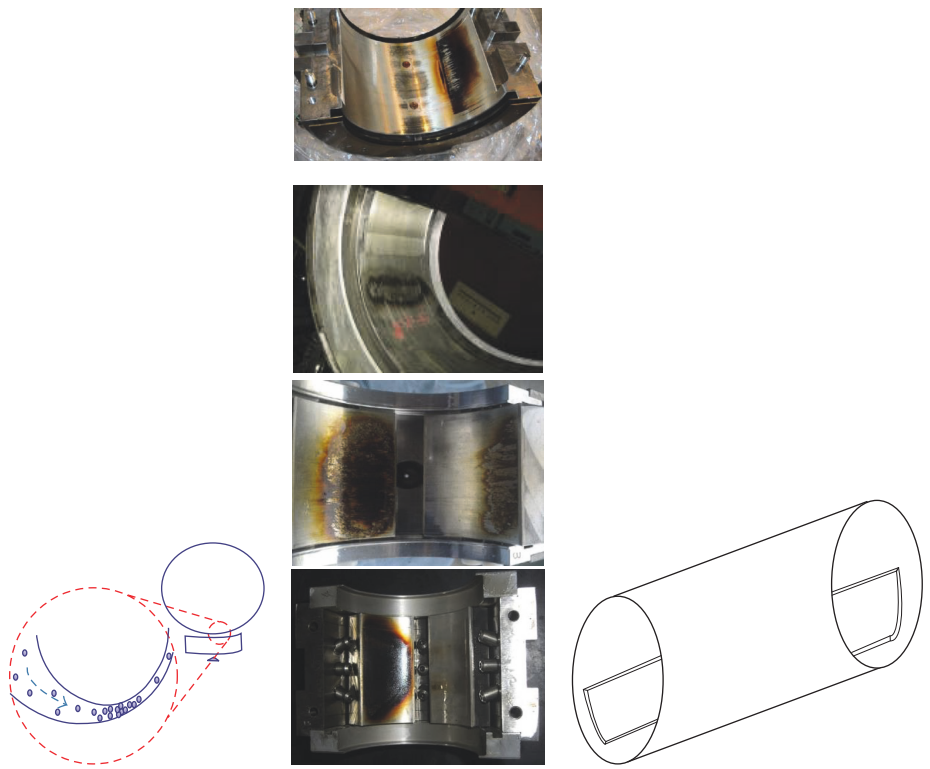

(a) Varnish location in the bearing (b) Varnish photographs (c) The simplified varnish model

Figure 1: Bearing varnish model.

varnish is a kind of protrusion on bearing inner face. It is mainly located in bearing load area, which is near the minimum gap and is the most dangerous zone of the bearing. Its influence on bearing performance may be large. Research in this field should be concerned.

In this paper, influences of varnish on bearing properties and rotor vibration are studied. Loading capacity, temperature rise, oil film thickness, and dynamic coefficients were compared. Conclusions can be applied to bearing condition monitoring.

## 2. Model of Bearing with Varnish

*2.1. Varnish Model.* Varnish is a kind of fouling adhered on journal bearing inner face nearby the load zone, as shown in Figure 1(a). Figure 1(b) shows 4 photographs of bearing with varnish.

For ease of analysis, varnish shape is simplified. A trapezoid distribution in the boundary and a uniform distribution in the inner face were assumed, as shown in Figure 1(c). This assumption guarantees continuity of the varnish at the boundary approximately.

Clearance of bearing with varnish can be expressed as [15]

$$H = 1 + \varepsilon \cos\varphi - H_1. \tag{1}$$

The partial derivative of clearance to circumferential angle is given by

$$\frac{\partial H}{\partial \varphi} = -\varepsilon \sin\varphi - \frac{\partial H_1}{\partial \varphi}. \tag{2}$$

*2.2. The Lubrication Equation.* A two-dimensional (2D) Reynolds equations were used. Taking into account the axial symmetry; the solution region was selected as the rectangular region ABCD, as shown in Figure 2. The varnish area is represented by a grid of lines in the figure.

The dimensionless form of the Reynolds equation is [15]

$$\frac{\partial}{\partial \varphi}\left(H^3 \frac{\partial P}{\partial \varphi}\right) + \left(\frac{d}{l}\right)^2 \frac{\partial}{\partial \lambda}\left(H^3 \frac{\partial P}{\partial \lambda}\right) = 3\frac{\partial H}{\partial \varphi}. \tag{3}$$

The Reynolds equation with the perturbation pressure $P_\varepsilon, P_\theta, P_{\varepsilon'}, P_{\theta'}$ as the variables is given as [16]

$$\frac{\partial}{\partial \varphi}\left(H^3 \frac{\partial P_\varepsilon}{\partial \varphi}\right) + \left(\frac{d}{l}\right)^2 \frac{\partial}{\partial \lambda}\left(H^3 \frac{\partial P_\varepsilon}{\partial \lambda}\right) = -3\sin\varphi - \frac{9}{H}$$

$$\cdot \cos\varphi \frac{\partial H}{\partial \varphi} + 3H\left[\left(\cos\varphi \frac{\partial H}{\partial \varphi} + \sin\varphi H\right)\frac{\partial P}{\partial \varphi}\right.$$

$$\left. + \left(\frac{d}{l}\right)^2 \cos\varphi \frac{\partial H}{\partial \lambda}\frac{\partial P}{\partial \lambda}\right] \frac{\partial}{\partial \varphi}\left(H^3 \frac{\partial P_\theta}{\partial \varphi}\right)$$

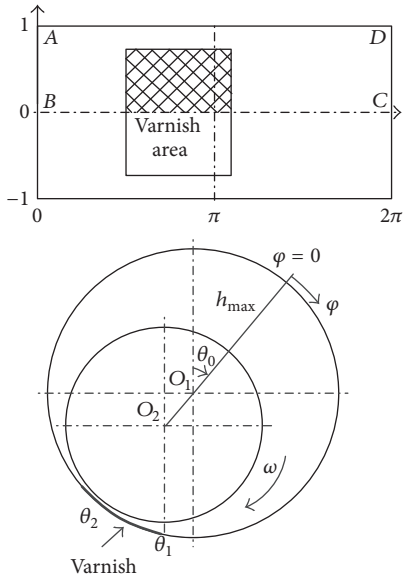


Figure 2: Lubrication equation solution model.

$$+\left(\frac{d}{l}\right)^2\frac{\partial}{\partial\lambda}\left(H^3\frac{\partial P_\theta}{\partial\lambda}\right)=3\cos\varphi$$
$$-\frac{9}{H}\sin\varphi\frac{\partial H}{\partial\varphi}+3H\left[\left(\sin\varphi\frac{\partial H}{\partial\varphi}-\cos\varphi H\right)\frac{\partial P}{\partial\varphi}\right.$$
$$\left.+\left(\frac{d}{l}\right)^2\sin\varphi\frac{\partial H}{\partial\lambda}\frac{\partial P}{\partial\lambda}\right]$$
$$\frac{\partial}{\partial\varphi}\left(H^3\frac{\partial P_{\varepsilon'}}{\partial\varphi}\right)+\left(\frac{d}{l}\right)^2\frac{\partial}{\partial\lambda}\left(H^3\frac{\partial P_{\varepsilon'}}{\partial\lambda}\right)=6\cos\varphi$$
$$\frac{\partial}{\partial\varphi}\left(H^3\frac{\partial P_{\theta'}}{\partial\varphi}\right)+\left(\frac{d}{l}\right)^2\frac{\partial}{\partial\lambda}\left(H^3\frac{\partial P_{\theta'}}{\partial\lambda}\right)=6\sin\varphi$$
$$P_\varepsilon=\frac{\partial P}{\partial\varepsilon},$$
$$P_\theta=\frac{\partial P}{\varepsilon\partial\theta},$$
$$P_{\varepsilon'}=\frac{\partial P}{\partial\varepsilon'},$$
$$P_{\theta'}=\frac{\partial P}{\varepsilon\partial\theta'}. \tag{4}$$

The boundary conditions of (3) and (4) are

$$P=P_\varepsilon=P_\theta=P_{\varepsilon'}=P_{\theta'}=0,\ \text{Line AB}$$
$$P=P_\varepsilon=P_\theta=P_{\varepsilon'}=P_{\theta'}=0,\ \text{Line CD}$$
$$P=P_\varepsilon=P_\theta=P_{\varepsilon'}=P_{\theta'}=0,\ \text{Line AD} \tag{5}$$
$$\frac{\partial P}{\partial\lambda}=\frac{\partial P_\varepsilon}{\partial\lambda}=\frac{\partial P_\theta}{\partial\lambda}=\frac{\partial P_{\varepsilon'}}{\partial\lambda}=\frac{\partial P_{\theta'}}{\partial\lambda}=0,\ \text{Line BC}.$$

During the iteration process, pressure is set to 0 if the negative pressure appears.

The varnish thickness is much smaller than the thickness of the pad. It has little influence on the heat conduction along the thickness direction of the pad. The heat conduction term was thus omitted. The simplistic two-dimensional energy equation with the adiabatic boundary condition is [13]

$$\rho\left[\left(\frac{Uh}{2}-\frac{h^3}{12\mu}\frac{\partial p}{\partial x}\right)\frac{\partial\left(c_vT\right)}{\partial x}-\frac{h^3}{12\mu}\frac{\partial p}{\partial z}\frac{\partial\left(c_vT\right)}{\partial z}\right]$$
$$=\mu\frac{U^2}{h}+\frac{h^3}{12\mu}\left[\left(\frac{\partial p}{\partial x}\right)^2+\left(\frac{\partial p}{\partial z}\right)^2\right]. \tag{6}$$

The symmetry boundary condition is adopted in the axis direction:

$$\frac{\partial T}{\partial\lambda}=0,\quad \lambda=0. \tag{7}$$

For the oil mixing condition at groove, the oil temperature is assumed as the mixing temperature between the recirculating oil and inlet oil. The average value of the recirculating temperature and the inlet oil temperature is taken as the mixing temperature. It is expressed as

$$T_{1,j}^{k+1}=\frac{T_{1,j}^k+T_{n,j}^k}{2}. \tag{8}$$

Lubricating oil viscosity variation with temperature is taken care of by the following expression [13]:

$$\mu=\mu_0e^{-\alpha(T-T_0)}. \tag{9}$$

Equations (3), (6), and (9) were solved by iterative method. Assuming the oil temperature distribution in the bearing, oil viscosity is calculated with (9) and oil film pressure is solved with (3). Substituting the calculated pressure into (6), the new temperature distribution is obtained. For the $k$th iteration process, initial temperature $T_{1,j}^k$ was known. Temperature $T_{i,j}^k$, $i=2,\ldots,n$ was calculated with (6) from the start angle to the end angle step by step. Then it was averaged using (8) to obtain the new temperature $T_{1,j}^{k+1}$. The iteration process stops when the solved temperature field is fully converged. The total iteration process stops when the solved pressure and temperature field are fully converged.

Bearing load is obtained by integral in axial and circumferential directions [15]:

$$F_x=-\frac{\mu\omega Rl}{(c/R)^2}\int_{\varphi_1}^{\varphi_2}\int_{-1}^{1}\left(p\mathrm{d}\lambda\right)\sin\varphi\,\mathrm{d}\varphi\,\mathrm{d}\lambda$$
$$F_y=-\frac{\mu\omega Rl}{(c/R)^2}\int_{\Phi_1}^{\Phi_2}\int_{-1}^{1}\left(p\mathrm{d}\lambda\right)\cos\varphi\,\mathrm{d}\varphi\,\mathrm{d}\lambda. \tag{10}$$

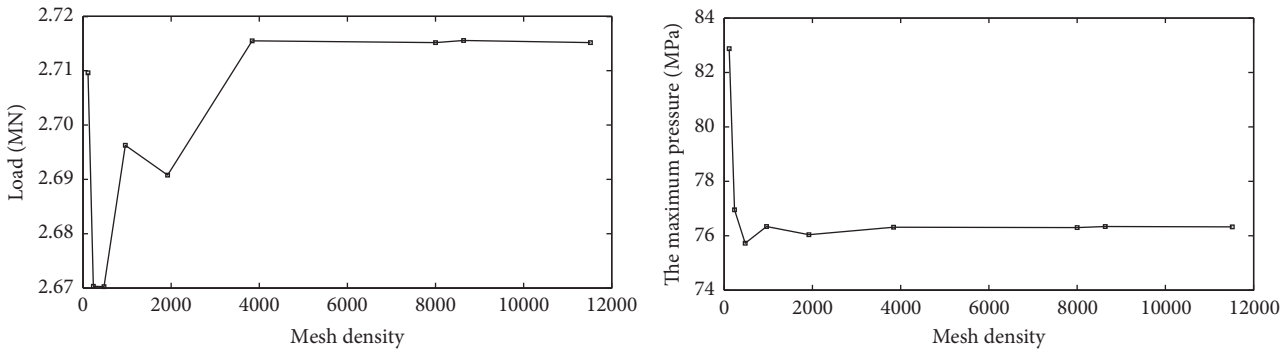


(a) Load (b) The maximum pressure

Figure 3: Variation of the load and the maximum pressure with mesh density.

The 8 dimensionless dynamic coefficients $K_{ij}, C_{ij},\ i, j = x, y$ can be calculated by [16]

$$\begin{bmatrix} K_{xx} & K_{xy} \\ K_{yx} & K_{yy} \end{bmatrix} = \begin{bmatrix} \sin\theta_0 & \cos\theta_0 \\ \cos\theta_0 & -\sin\theta_0 \end{bmatrix} \cdot \begin{bmatrix} K_{ee} & K_{\theta e} \\ K_{e\theta} & K_{\theta\theta} \end{bmatrix} \cdot \begin{bmatrix} \sin\theta_0 & \cos\theta_0 \\ \cos\theta_0 & -\sin\theta_0 \end{bmatrix}$$

$$\begin{bmatrix} C_{xx} & C_{xy} \\ C_{yx} & C_{yy} \end{bmatrix} = \begin{bmatrix} \sin\theta_0 & \cos\theta_0 \\ \cos\theta_0 & -\sin\theta_0 \end{bmatrix} \cdot \begin{bmatrix} C_{ee} & C_{\theta e} \\ C_{e\theta} & C_{\theta\theta} \end{bmatrix} \cdot \begin{bmatrix} \sin\theta_0 & \cos\theta_0 \\ \cos\theta_0 & -\sin\theta_0 \end{bmatrix}$$

$$\begin{Bmatrix} K_{ee} \\ K_{\theta e} \end{Bmatrix} = -\int_{-1}^{1}\int_{\varphi_1}^{\varphi_2} P_{\varepsilon} \begin{Bmatrix} \cos\varphi \\ \sin\varphi \end{Bmatrix} d\varphi\, d\lambda$$

$$\begin{Bmatrix} K_{e\theta} \\ K_{\theta\theta} \end{Bmatrix} = -\int_{-1}^{1}\int_{\varphi_1}^{\varphi_2} P_{\theta} \begin{Bmatrix} \cos\varphi \\ \sin\varphi \end{Bmatrix} d\varphi\, d\lambda$$

$$\begin{Bmatrix} C_{ee} \\ C_{\theta e} \end{Bmatrix} = -\int_{-1}^{1}\int_{\varphi_1}^{\varphi_2} P_{\varepsilon'} \begin{Bmatrix} \cos\varphi \\ \sin\varphi \end{Bmatrix} d\varphi\, d\lambda$$

$$\begin{Bmatrix} C_{e\theta} \\ C_{\theta\theta} \end{Bmatrix} = -\int_{-1}^{1}\int_{\varphi_1}^{\varphi_2} P_{\theta'} \begin{Bmatrix} \cos\varphi \\ \sin\varphi \end{Bmatrix} d\varphi\, d\lambda. \quad (11)$$

*2.3. Grid Independence Test.* The computational accuracy depends on mesh density. The load and the maximum pressure were used to test grid independence. With the increase of journal eccentricity ratio in the bearing, mesh density should be increased. Thus, the grid independence test was done at large eccentricity ratio $\varepsilon = 0.90$.

Table 1 gives bearing data. Figure 3 shows variation of the load and the maximum pressure with the mesh density. When the grid density is greater than 4000, the load and the maximum pressure change a little. To ensure the accuracy, mesh with 60 in the axial direction by 180 in the circumferential direction was used at last.

Table 1: Bearing data.

| Parameter | Value |
|---|---|
| Radius $R$ | 300 mm |
| Radial clearance $c$ | 0.45 mm |
| Bearing length $l$ | 300 mm |
| Bearing load $F_y$ | 20.0 t |
| Oil density $\rho$ | 890 kg/m$^3$ |
| Oil viscosity $\mu$ | 0.025 Pa s |
| Rotating speed $\omega$ | 314 rad/s |
| Specific heat capacity $c_v$ | 1.944 kJ/kg K |

*2.4. Journal Position in the Bearing.* Oil film force at different eccentricity ratio and attitude angle was calculated in advance. The back propagation neural network is well known for its strong nonlinear mapping ability. A three-layer backpropagation neural network with 8 nodes in the hidden layer, as shown in Figure 4, was trained to map the functional relationship between the force and the journal position in the bearing. The input of the neural network is bearing load in the horizontal and the vertical directions. The output of the neural network is journal eccentricity ratio and the attitude angle. For improving mapping accuracy, neural network for small bearing load case and for large bearing load case was trained, respectively. Once the bearing load is given, the position of the journal in the bearing can be calculated easily.

## 3. Influence of Varnish on Bearing Performance

Bearing data is provided in Table 1. In the analysis, the dimensionless thickness of the varnish is changed from 0.0 to 0.3. Varnish is located in the load zone. The leading edge angle and the trailing edge angle are 165° and 192° and the arc length of varnish is about 27°. Influence of varnish on bearing performance was carried out assuming that bearing load is the same.

*3.1. Oil Film Thickness.* Figure 5 compares oil film thickness distribution in the central section along the circumferential direction for bearing with and without varnish. Figure 6

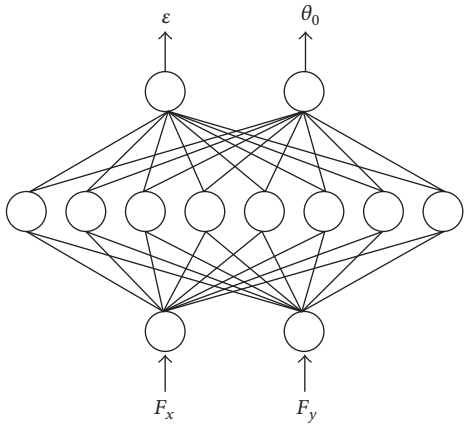


Figure 4: Neural network model mapping the function between the force and journal position.

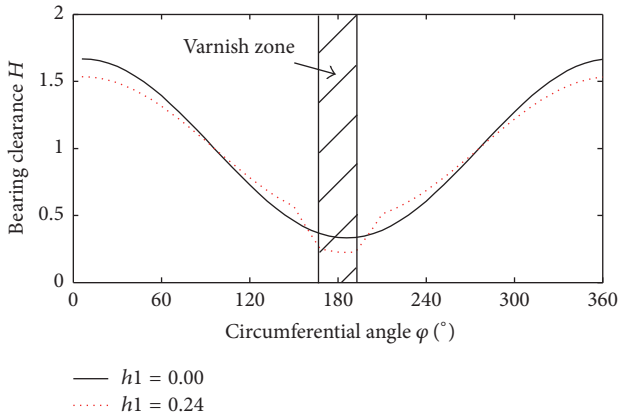


Figure 5: Oil film thickness distribution.

shows variation of the minimum oil film thickness with varnish thickness. The oil film thickness is smaller in the varnish zone. The minimum oil film thickness decreases with the increase of varnish thickness.

*3.2. Bearing Pressure Distribution.* Figure 7 compares oil film pressure distribution for bearings. Beyond the varnish zone, oil pressure increases gradually under the effect of squeeze film formed in the converged region of the bearing. At the leading edge of the varnish, the step flow effect is formed for that bearing clearance becomes smaller suddenly. The pressure increases quickly and the maximum pressure appears. The performance of bearing with vanish depends on the joint action of the squeeze film effect and the step flow effect.

*3.3. Journal Position.* Figure 8 shows variation of journal eccentricity ratio with bearing load. Journal eccentricity ratio of bearing without varnish is larger because that bearing load is supported by the squeeze film effect only. Figure 9 shows variation of journal eccentricity ratio with varnish thickness. Figure 10 shows variation of the eccentricity ratio and the attitude angle with rotational speed. For bearing with varnish, bearing load is partially compensated by the step flow effect

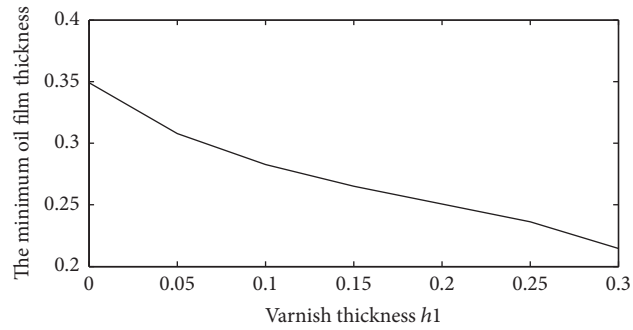


Figure 6: Variation of the minimum oil film thickness with varnish thickness.

caused by the varnish. So, the thicker the varnish, the smaller the journal eccentricity ratio and the larger the attitude angle.

*3.4. Bearing Temperature.* Figure 11 compares temperature distribution of bearing with different varnish thickness. Oil film temperature increases quickly at the leading edge of the varnish and reaches the maximum value at the trailing edge. Figure 12 shows variation of the maximum oil temperature with varnish thickness. The maximum oil temperature increases with the increase of varnish thickness. In the early stage of the varnish, temperature growth trend is slow. However, the trend of temperature increasing is more and more obvious with the increase of thickness.

Figure 13 shows temperature trend in a year for the third bearing of Figure 1(b). Although the bearing temperature is not high, the trend of growth is obvious. And the temperature is getting higher and higher. Bearing was overhauled for inspection. Vanish is found on the inner surface of the bearing, as shown in Figure 1(b). The temperature increase phenomenon found in the bearing is almost similar to the simulated result of Figure 12.

*3.5. Loading Capacity.* Figure 14 shows the variation of the minimum clearance with bearing load. With the increase of varnish thickness, the load corresponding to the same minimum clearance decreases. It means that loading capacity of bearing with varnish is smaller than that of bearing without varnish.

Varnish in the bearing results in a large decrease of minimum clearance and an increase in the oil film temperature and the pressure. Loading capacity of bearing is decreased. It is harmful to the safe operation of bearing.

*3.6. Bearing Dynamic Coefficients.* Figure 15 shows the variation of bearing stiffness and damping coefficients with frequency. The stiffness and the damping coefficients are larger for bearing with varnish. Its influence is larger in the horizontal direction than that in the vertical direction. The dynamic pressure effect caused by the step flow is relatively large at low speed. This leads to the greater impact on bearing dynamics at low speed.

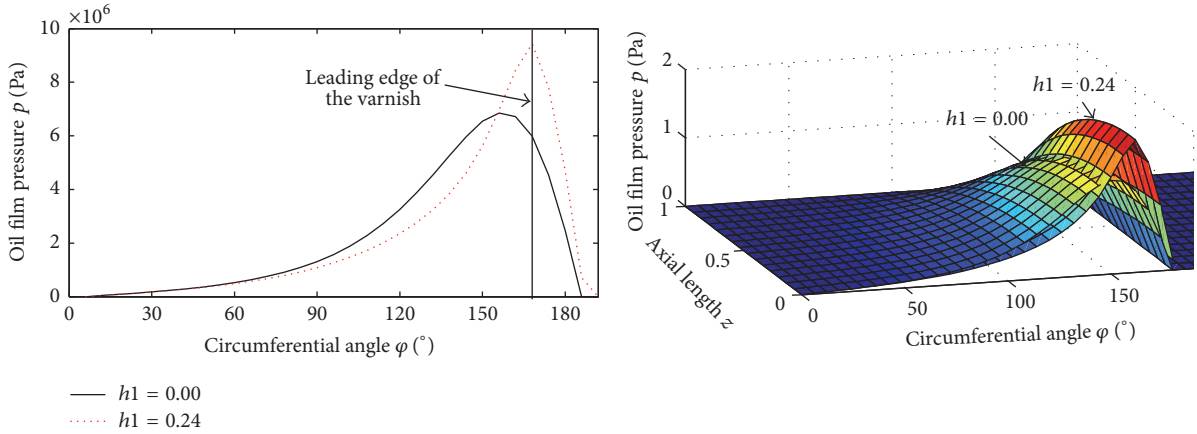


(a) Pressure distribution in the central section

(b) The three-dimensional pressure distribution

Figure 7: Oil film pressure distribution.

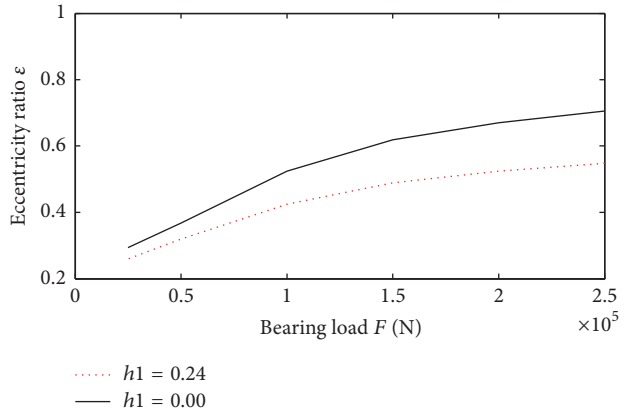


Figure 8: Variation of journal eccentricity ratio with bearing load.

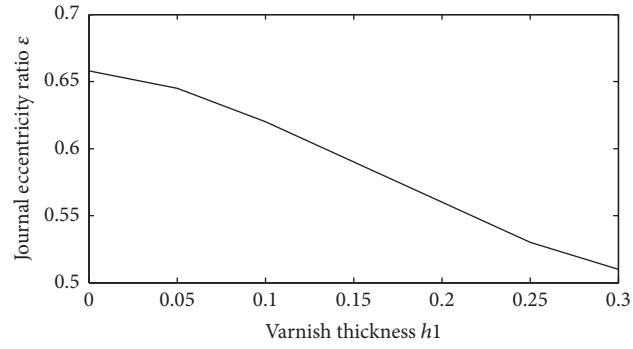


Figure 9: Variation of journal eccentricity ratio with varnish thickness.

For stability study, bearing equivalent stiffness and critical whirl ratio can be presented using bearing coefficients. They are given as [17]

$$K_{\text{eq}} = \frac{K_{xx}C_{yy} + K_{yy}C_{xx} - K_{xy}C_{yx} - K_{yx}C_{xy}}{C_{xx} + C_{yy}}$$
$$\gamma_{\text{st}}^2 = \frac{\left(K_{xx} - K_{\text{eq}}\right)\left(K_{yy} - K_{\text{eq}}\right) - K_{xy}K_{yx}}{C_{xx}C_{yy} - C_{xy}C_{yx}}. \quad (12)$$

The calculation results are given in Table 2. For bearings studied in the case, $K_{\text{eq}} > 0$, $\gamma_{\text{st}}^2 < 0$. It means that bearings are stable. However, for bearings with varnish, its equivalent stiffness is higher and its critical whirl ratio is lower. It means that varnish has certain positive effect on bearing stability.

Table 2: Bearing equivalent stiffness and critical whirl ratio.

| Parameter | With varnish | Without varnish |
|---|---|---|
| Equivalent stiffness | 1.8314 | 1.7542 |
| Critical whirl ratio | −0.2956 | −0.2146 |

## 4. Influence of Varnish on Rotor Unbalance Response and System Stability

*4.1. Dynamic Equation.* The dynamic equation of rotor bearing system is given as [18]

$$[\mathbf{M}]\left\{\ddot{\mathbf{U}}(t)\right\} + [\mathbf{D}]\left\{\dot{\mathbf{U}}(t)\right\} + [\mathbf{K}]\{\mathbf{U}(t)\} = \{\mathbf{F}(t)\}. \quad (13)$$

Assume that

$$\mathbf{U}(t) = \mathbf{U}_0(t)\, e^{i\omega t}$$
$$\mathbf{F}(t) = \mathbf{F}_0(t)\, e^{i\omega t}. \quad (14)$$

Substituting (14) into (13), we can get

$$\left[\mathbf{K} + i\omega\mathbf{D} - \omega^2\mathbf{M}\right]\{\mathbf{U}_0\} = \{\mathbf{F}_0\}. \quad (15)$$

The unbalance response can be calculated with the equation.

The homogeneous equation corresponding to (13) can be written as

$$[\mathbf{M}]\left\{\ddot{\mathbf{U}}(t)\right\} + [\mathbf{D}]\left\{\dot{\mathbf{U}}(t)\right\} + [\mathbf{K}]\{\mathbf{U}(t)\} = \{\mathbf{0}\}. \quad (16)$$

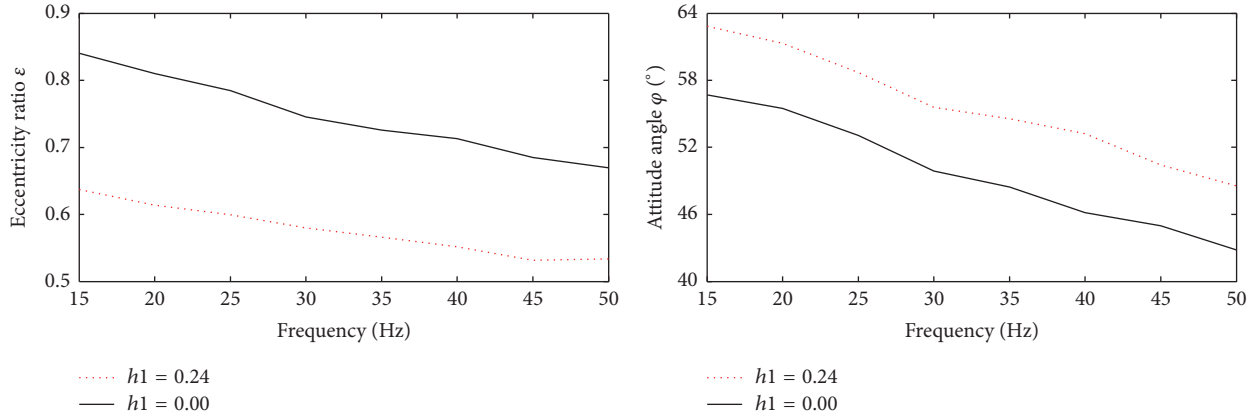


(a) The eccentricity ratio (b) The attitude angle

Figure 10: Comparison of journal eccentricity ratio and attitude angle.

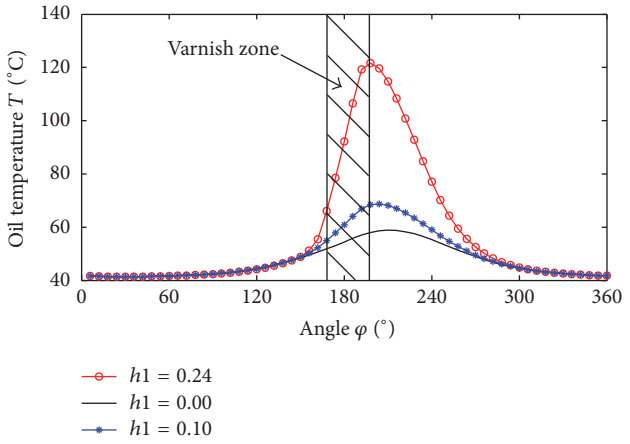


Figure 11: Comparison of temperature distribution.

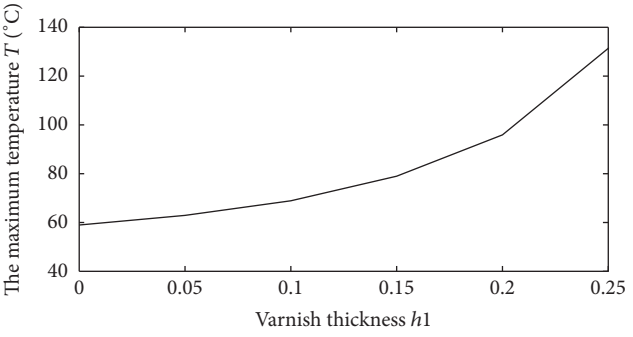


Figure 12: Variation of the maximum oil temperature with varnish thickness.

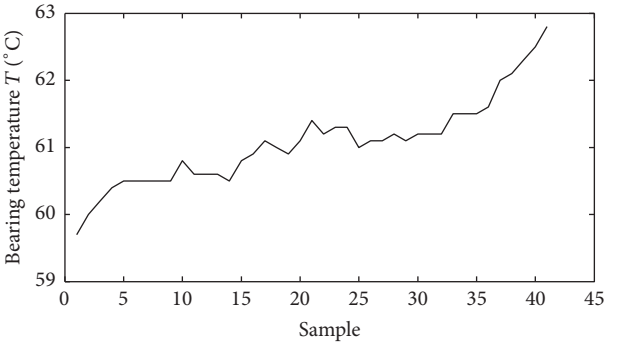


Figure 13: Bearing temperature trend in a year.

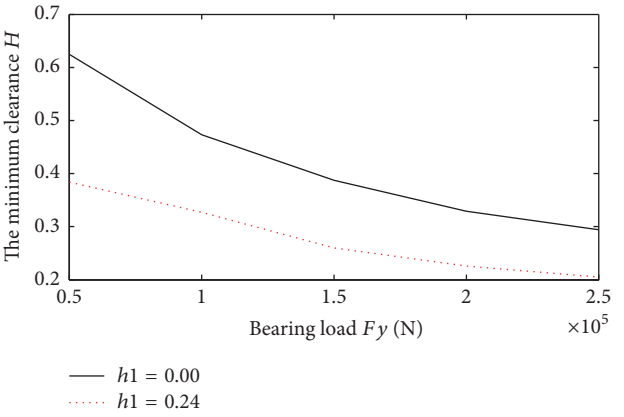


Figure 14: Variation of the minimum oil film thickness with bearing load.

The first-order differential equations of (16) are

$$[\mathbf{A}]\left\{\dot{\mathbf{V}}\right\} + [\mathbf{B}]\{\mathbf{V}\} = \{\mathbf{0}\}$$

$$\mathbf{A} = \begin{bmatrix} \mathbf{M} & \mathbf{0} \\ \mathbf{0} & \mathbf{K} \end{bmatrix},$$

$$\mathbf{B} = \begin{bmatrix} \mathbf{D} & \mathbf{K} \\ -\mathbf{K} & \mathbf{0} \end{bmatrix},$$

$$\mathbf{V} = \begin{Bmatrix} \dot{\mathbf{U}} \\ \mathbf{U} \end{Bmatrix}. \tag{17}$$

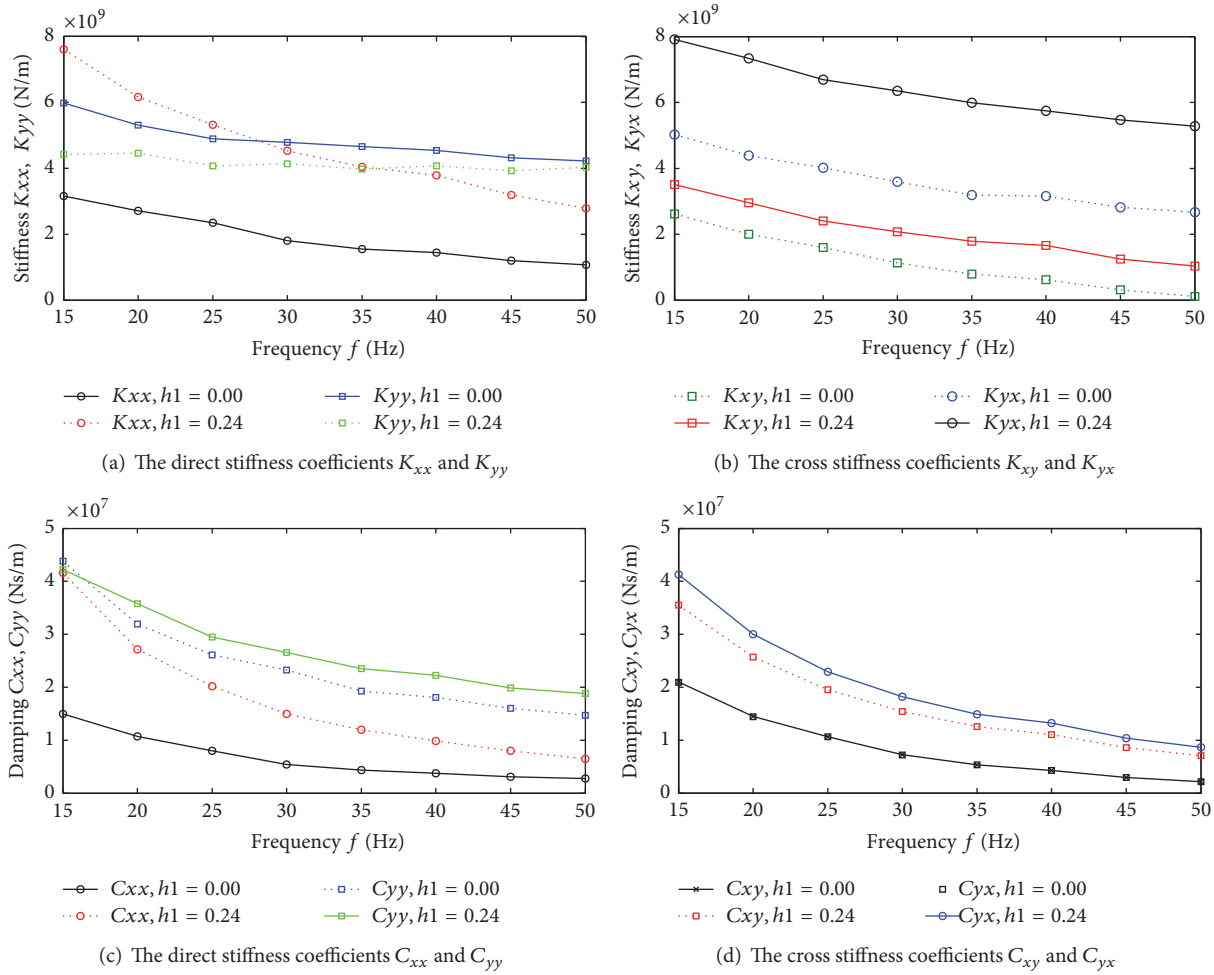


(a) The direct stiffness coefficients $K_{xx}$ and $K_{yy}$

(b) The cross stiffness coefficients $K_{xy}$ and $K_{yx}$

(c) The direct stiffness coefficients $C_{xx}$ and $C_{yy}$

(d) The cross stiffness coefficients $C_{xy}$ and $C_{yx}$

FIGURE 15: Comparison of bearing dynamic coefficients.

The eigenvalues and eigenvectors are

$$(\mathbf{E} - \nu\mathbf{I})\,\mathbf{V}_0 = \mathbf{0}$$

$$\mathbf{E} = \begin{bmatrix} -\mathbf{M}^{-1}\mathbf{D} & -\mathbf{M}^{-1}\mathbf{K} \\ \mathbf{I} & \mathbf{0} \end{bmatrix}. \tag{18}$$

The stability of the system is represented by the logarithmic decrement rate $\delta$. It can be calculated from system eigenvalue $\nu$:

$$\delta = -2\pi \frac{\Re(\nu)}{\Im(\nu)}. \tag{19}$$

The greater the value $\delta$ is, the more stable the system is. In order to ensure the stability of the system, $\delta \geq 0.2$.

*4.2. Model of a Low Pressure Rotor.* A low pressure rotor of a large steam turbine was used. Figure 16 shows the model. Bearing data is provided in Table 1. Shaft data is given in Table 3. Considering the axial symmetry, only half of the shaft data is given.

*4.3. Unbalance Response Analysis.* Three unbalance masses as shown in Table 4 were exerted on the rotor. The first and the third set of masses represent the coupled unbalance and the second set of mass represents the static unbalance in the middle plane.

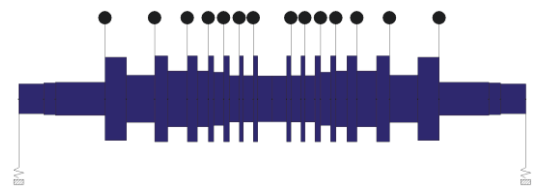

FIGURE 16: Shaft model.

The influence of varnish on the vertical and the horizontal vibration during the run up process is shown in Figure 17. For bearing with varnish or without varnish, the trend of the response to rotating speed is similar. Influence of varnish on the horizontal vibration is larger than that on the vertical vibration, especially in the low speed zone. This is consistent with the influence of the varnish on bearing dynamic characteristics. The damping coefficient in the horizontal direction of the bearing with varnish is large. Its effect on vibration control near the first critical speed zone is obvious.

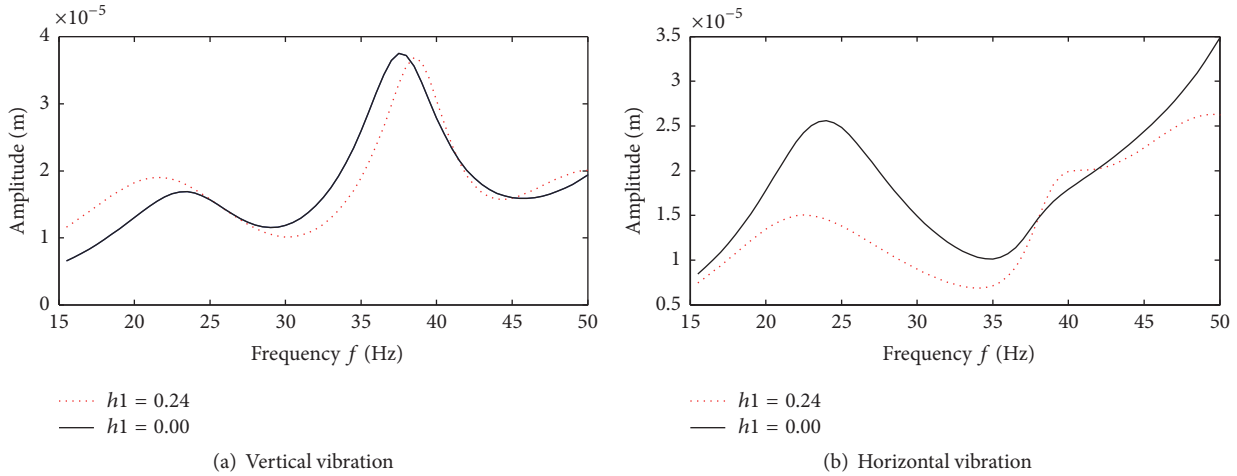


(a) Vertical vibration (b) Horizontal vibration

Figure 17: Variation of vibration with rotating speed during run-up process.

Table 3: Shaft model.

| Diameter $D$ (mm) | Length $L$ (mm) | Additional mass $M$ (kg) |
|---|---|---|
| 600 | 300 | 0 |
| 630 | 142 | 0 |
| 660 | 594 | 0 |
| 1668 | 256 | 1850 |
| 951 | 340 | 0 |
| 1720 | 156 | 900 |
| 1116 | 236 | 0 |
| 1718 | 120 | 300 |
| 1114 | 130 | 0 |
| 1718 | 65 | 280 |
| 1068 | 120 | 0 |
| 1718 | 66 | 180 |
| 934 | 120 | 0 |
| 1718 | 50 | 110 |
| 934 | 120 | 0 |
| 1718 | 50 | 100 |
| 915 | 175 | 0 |

Table 4: Unbalance mass.

| Node | Product of mass and radius (kg m) | Angle (°) |
|---|---|---|
| 4 | 0.5 | 45 |
| 17 | 1 | 135 |
| 32 | 0.5 | 225 |

*4.4. System Stability.* The lowest order modes are prone to be unstable and are of great concern. In this paper, stability of the first and the second mode is analyzed.

Table 5 shows the influence of the varnish on system stability. Influence of the varnish on modal frequency is small. However, system stability is improved due to the increased bearing damping coefficients. The conclusion is the same as that in Section 3.6.

Table 5: Comparison of system stability.

| Mode | Parameter | With varnish | Without varnish |
|---|---|---|---|
| Mode 1 | Frequency/Hz | 23.48 | 23.31 |
| | Logarithmic decrement rate | 0.5029 | 0.4645 |
| Mode 2 | Frequency/Hz | 34.45 | 34.41 |
| | Logarithmic decrement rate | 0.5327 | 0.4614 |

## 5. Conclusions

In this paper, the influence of the varnish on bearing performance and rotor vibration is studied. The results show the following.

(1) Performance of bearing with varnish is changed by the step flow effect at the leading edge of the varnish. Compared with the squeeze flow effect in the convergent clearance zone of bearing, influence of varnish is more obvious at the low speed case.

(2) Varnish in the bearing results in a large decrease of minimum clearance and an increase in the oil film temperature and the pressure. Loading capacity of bearing is also decreased. It is harmful to the safe and reliable operation of bearing.

(3) For bearing with varnish, the minimum oil film thickness decreases. This leads to an increase of bearing stiffness and damping coefficients. Its influence is larger in the horizontal direction than that in the vertical direction.

(4) For bearing with varnish or without varnish, the trend of the response to rotating speed is similar. Its Influence on the horizontal vibration is larger than that on the vertical vibration, especially in the low speed zone. This is consistent with the influence of the varnish on bearing dynamic

characteristics. There is little influence of the varnish on the modal frequency. However, system stability is improved due to the increased bearing damping coefficients.

## Nomenclature

*Symbols*

| | |
|---|---|
| $H$: | Dimensionless bearing clearance |
| $h$: | Dimensional bearing clearance |
| $H_1$: | Dimensionless varnish thickness |
| $\varphi$: | Circumferential angle |
| $\varepsilon$: | Journal eccentricity ratio |
| $e$: | Journal eccentricity |
| $\theta_0$: | Journal attitude angle |
| $c$: | Bearing radial gap |
| $d$: | Bearing diameter |
| $R$: | Bearing radius |
| $l$: | Bearing length |
| $\lambda$: | Bearing axial dimensionless coordinate |
| $P$: | Dimensionless oil pressure |
| $p$: | Dimensional oil pressure |
| $P_\varepsilon, P_\theta, P_{\varepsilon'}, P_{\theta'}$: | Perturbation oil pressure |
| $T$: | Oil temperature |
| $\rho$: | Oil density |
| $\mu$: | Oil viscosity |
| $\alpha$: | Oil viscosity coefficient |
| $c_v$: | Specific heat capacity |
| $U$: | Journal velocity |
| $F_x, F_y$: | Bearing loads in horizontal and vertical direction |
| $K_{ij}$: | Bearing stiffness coefficients |
| $C_{ij}$: | Bearing damping coefficients |
| $K_{\text{eq}}$: | Bearing equivalent stiffness |
| $\gamma_{\text{st}}$: | Critical whirling ratio |
| $\omega$: | Rotating speed |
| $\delta$: | Logarithmic decrement rate |
| **M**, **K**, **D**: | System mass, stiffness, and gyroscopic/damping matrices |
| **U**: | Degree of freedom vector |
| **F**: | External force vector |
| $\boldsymbol{\nu}$: | System eigenvalues |
| $\mathbf{V}_0$: | System eigenvectors |
| $\mathbf{U}_0$: | Amplitude of displacement vector |
| $\mathbf{F}_0$: | Amplitude of the forces vector |
| $\mathfrak{R}(\cdot)$: | Real part of variable |
| $\mathfrak{I}(\cdot)$: | Imaginary part of variable. |

## Conflicts of Interest

The authors declare that there are no conflicts of interest regarding the publication of this paper.

## References


[1] F. Yokoyama, Y. Iwama, M. Maruyama, and M. Sano, "Deposits on bearing pad caused by particulate contamination in turbine oil," *Tribology Online*, vol. 10, no. 2, pp. 162–171, 2015.

[2] A. Yano, S. Watanabe, Y. Miyazaki, M. Tsuchiya, and Y. Yamamoto, "Study on sludge formation during the oxidation process of turbine oils," *Tribology Transactions*, vol. 47, no. 1, pp. 111–122, 2004.

[3] A. Sasaki, S. Uchiyama, and M. Kawasaki, "Varnish formation in the gas turbine oil systems," *Journal of ASTM International*, vol. 5, no. 2, 2008.

[4] T. V. V. L. N. Rao, A. M. A. Rani, T. Nagarajan, and F. M. Hashim, "Analysis of slider and journal bearing using partially textured slip surface," *Tribology International*, vol. 56, pp. 121–128, 2012.

[5] N. Tala-Ighil and M. Fillon, "A numerical investigation of both thermal and texturing surface effects on the journal bearings static characteristics," *Tribology International*, vol. 90, pp. 228–239, 2015.

[6] C. Sinanoğlu, F. Nair, and M. B. Karamış, "Effects of shaft surface texture on journal bearing pressure distribution," *Journal of Materials Processing Technology*, vol. 168, no. 2, pp. 344–353, 2005.

[7] F. M. Meng and T. Yang, "Preliminary study on mechanism of cavitation in lubricant of textured sliding bearing," *Proceedings of the Institution of Mechanical Engineers, Part J: Journal of Engineering Tribology*, vol. 227, no. 7, pp. 695–708, 2013.

[8] M. Qiu, B. R. Minson, and B. Raeymaekers, "The effect of texture shape on the friction coefficient and stiffness of gas-lubricated parallel slider bearings," *Tribology International*, vol. 67, pp. 278–288, 2013.

[9] A. De Kraker, R. A. J. Van Ostayen, and D. J. Rixen, "Development of a texture averaged Reynolds equation," *Tribology International*, vol. 43, no. 11, pp. 2100–2109, 2010.

[10] C. B. Khatri and S. C. Sharma, "Influence of textured surface on the performance of non-recessed hybrid journal bearing operating with non-Newtonian lubricant," *Tribology International*, vol. 95, pp. 221–235, 2016.

[11] N. Tala-Ighil, M. Fillon, and P. Maspeyrot, "Effect of textured area on the performances of a hydrodynamic journal bearing," *Tribology International*, vol. 44, no. 3, pp. 211–219, 2011.

[12] F. M. Meng, L. Zhang, and T. Long, "Effect of Groove Textures on the Performances of Gaseous Bubble in the Lubricant of Journal Bearing," *Journal of Tribology*, vol. 139, no. 3, Article ID 031701, 2017.

[13] S. Kango, R. K. Sharma, and R. K. Pandey, "Comparative analysis of textured and grooved hydrodynamic journal bearing," *Proceedings of the Institution of Mechanical Engineers, Part J: Journal of Engineering Tribology*, vol. 228, no. 1, pp. 82–95, 2014.

[14] J. Dong, X. Wang, and J. Zhang, "An experimental research on the vibration of surface-textured journal bearings," *Shock and Vibration*, vol. 2017, Article ID 1261826, 9 pages, 2017.

[15] V. Brizmer and Y. Kligerman, "A laser surface textured journal bearing," *Journal of Tribology*, vol. 134, no. 3, Article ID 031702, 2012.

[16] O. Ebrat, Z. P. Mourelatos, N. Vlahopoulos, and K. Vaidyanathan, "Calculation of journal bearing dynamic characteristics including journal misalignment and bearing structural deformation," *Tribology Transactions*, vol. 47, no. 1, pp. 94–102, 2004.

[17] C. Y. Chen, R. H. Yen, and C. S. Liu, "Characteristics of dynamic coefficients on stability for herringbone-grooved journal bearings," *Applied Mathematics & Information Sciences*, vol. 7, no. 3, pp. 1215–1223, 2013.

[18] K. L. Cavalca, P. F. Cavalcante, and E. P. Okabe, "An investigation on the influence of the supporting structure on the dynamics of the rotor system," *Mechanical Systems and Signal Processing*, vol. 19, no. 1, pp. 157–174, 2005.